

Amoeboid swimming in a channel

Hao Wu,^{1,2} A. Farutin,^{1,2} W.-F. Hu,³ M. Thiébaud,^{1,2} S. Rafaï,^{1,2} P. Peyla,^{1,2} M.-C. Lai,⁴ and C. Misbah^{1,2}

¹Université Grenoble Alpes, LIPHY, F-38000 Grenoble, France

²CNRS, LIPHY, F-38000 Grenoble, France

³Department of Applied Mathematics, National Chung Hsing University, 145 Xingda Road, Taichung 402, Taiwan

⁴Department of Applied Mathematics, National Chiao Tung University, 1001 Ta Hsueh Road, Hsinchu 300, Taiwan

Several micro-organisms, such as bacteria, algae, or spermatozoa, use flagellum or cilium activity to swim in a fluid. Many other organisms use rather ample shape deformation, described as *amoeboid*, to propel themselves, either crawling on a substrate or swimming. Many eukaryotic cells were believed to require an underlying substratum to migrate (crawl) by using ample membrane deformation (like blebbing, or generation of lamellipodia). There is now an increasing evidence that a large variety of cells (including those of the immune system) can migrate without the assistance of focal adhesion, and can perform swimming as efficiently as crawling. This paper deals with a detailed analysis of amoeboid swimming in a confined fluid, by modeling the swimmer as an inextensible membrane deploying local active forces (with zero total force and torque). The swimmer exhibits a rich behavior: it can settle into a straight trajectory in the channel, or can navigate from one wall to the other, depending on confinement. Furthermore, the nature of the swimmer is found to be affected by the confinement: the swimmer can behave as a pusher at low confinement, and becomes a puller at higher confinement, or vice versa; this shows that the swimmer nature is not an intrinsic property. The scaling of the swimmer velocity V with the force amplitude A is analyzed in details and this shows that at small enough A , $V \sim A^2/\eta^2$ (where η is the viscosity of the ambient fluid), whereas at large enough A , V is independent of the force and is only fixed by the stroke cycle frequency and the swimmer size. This finding markedly contrasts with results known for swimming models referring to motion based on cilium and flagellum activity where $V \sim A/\eta$. Two types of efficiencies, put forward in the literature, are analyzed and it is found that the outcomes from each definition are quite distinct. We find that one type of efficiency has an optimum at a given confinement while the other has none. Future perspectives are outlined.

I. INTRODUCTION

In the past decade, the problem of swimming in low Reynolds number environment has attracted much attention from biology, physics, applied mathematics, computer science, chemistry, and mechanical engineering. Many kinds of motile unicellular micro-organisms living in the world of low Reynolds number [1, 2] use a variety of strategies to propel themselves in liquids. So far most of the studies have been directed towards organisms employing flagellum and cilium activity. Typical examples are spermatozoa [3, 4], bacteria such as *E. coli* [5, 6] and *Bacillus subtilis* [7] (examples of the so-called pusher), algae like *Chlamydomonas Reinhardtii* (an example of puller) [4, 8, 9], *Volvox* [8, 10] and *Paramecium* [11, 12] (examples of neutral swimmers). There has been also a great interest in designing artificial microswimmers driven by different external fields, such as a rotating magnetic field [13], a catalytic reaction field [14], and so on.

Another category of swimmers, which has been much less studied so far, and constitutes now an emerging activity is that related to amoeboid swimming (AS), a motility based on ample shape deformation. Amoeboid movement is the most common mode of locomotion in eukaryotic cells (monocytes, neutrophils, macrophages, cancerous cells, etc.). The denomination *amoeboid motion* generically refers to motility performed thanks to shape deformation. Actually amoeboid motion can be

performed in a solution (like swimming) or on a substratum (crawling). A prototypical example of the first category is *Eutreptiella Gymnastica* [15], a common representative of euglenids of marine phytoplankton. Many eukaryotic cells, such as leucocytes, fibroblasts, etc., use ample membrane deformation for motility, but were often categorized as microorganisms that must use focal adhesion on a substratum to move forward. This type of motion is often referred as *crawling* too. The crawling problem has been extensively studied in the biological and biophysical literatures [16, 17]. Crawling plays an essential role in many physiological and pathological processes, including embryonic development, wound healing, immune response and cancer metastasis. Several recent studies have been directed towards elucidating more deeply the role of focal adhesion in the migration process. Recent studies revealed that adhesion-based crawling is not necessarily a pre-requisite for cell locomotion once leukocytes transmigrate across the endothelium [18]. Adhesion molecules would only serve to stop moving leukocytes in the blood stream, making them adhering to the endothelium before transmigration. Studies *in vitro* have shown that integrins (principal cell adhesion molecules) do not contribute to migration in three-dimensional environments (in suspension with fibrous material, mimicking extracellular matrix of tissues)[18]. Instead, these cells migrate by the sole force of actin-network expansion, which promotes protrusive flowing of the leading edge. It seems debated[19, 20] whether or not the contact of the cell with the fibrous material, albeit without

specific adhesion, is necessary in order to assist locomotion. A more recent study supports the idea of a pure swimming of cells of the immune systems (neutrophils), and of dictyostelium [21]. It has been found that these cells move toward a chemotactic source while suspended in solution. They can swim and do so with speeds similar to those on a solid substrate (crawling). More recent experimental studies have focused [22] on cell motion in a confined geometry and showed that a blebbing cell[55] can undergo movement through nonspecific adhesion, but only thanks to a solid-like friction from the substrate. In other words, this corresponds to a situation where the cell is in "physical" contact with the substrate on which the cell might lean, in a similar fashion as with the case of a cell leaning on a fibrous (or extracellular material), but no specific adhesion is needed.

The above studies lend strong support to the idea that adhesion is not necessary for migration. In some reported cases [21] cells can even bypass contact with substrate and perform pure swimming in a fluid. There seems thus to be a whole spectrum of possibilities that can be relevant for cell migration, ranging from specific-adhesion assisted crawling, through pure non specific friction with elastic substratum, up to pure swimming in a solution. It is thus an important task of investigation to attempt bridging the gap between pure swimming and motion through physical contacts (solid-like friction) up to crawling.

The present goal is to first isolate different effects and progressively increase the degree of complexity in order to unravel the imbricated nature of cell motility. Therefore, we have systematically analyzed amoeboid motion in the pure swimming case, and have studied the effect of bounding walls. Though there is no direct friction (no contact) with walls, the fluid in the gap between the swimmer and the walls serves as a support to transmit friction forces between the swimmer and the walls.

Several models of directed self-propulsion by large shape deformation have been explored in the literature [23–31]. In two recent studies we have introduced a model in which [30, 31] the swimmer is considered as made of an inextensible membrane enclosing a constant volume of liquid and exerting a set of normal forces leading to deformations of the swimmer and to propulsion. The first study [30] has dealt with purely unconfined three dimensional (3D) geometry, and a more recent work was dedicated to a confined swimmer in two dimensions (2D) [31], a situation which has revealed several puzzling phenomena, as will be recalled hereafter. Here we report on several new issues emerging for a confined amoeboid swimmer. For example, we show that the velocity of migration has a nontrivial scaling with the force. We also address the notion of efficiency by using two types of definitions. We shall see, for example, that the efficiency exhibits an optimum at a bifurcation point where the swimmer exhibits a transition from a pusher to a puller-type. We will discuss the space scanning capability of the swimmer, where we find that generally the swimmer

can scan about 90% of the available space.

This paper is organized as follows: In Section II, we present a minimal model for AS. In Section III the two numerical methods used in this study are briefly recalled: the boundary integral method (BIM) [31, 32] and the immersed boundary method (IBM) [33]. In Section IV, we present the main results regarding an axially moving swimmer. In Section V we discuss both the peculiar behavior of the velocity as a function of confinement and the power consumption problem. Section VI analyzes the swimmer efficiency. Section VII is devoted to the different dynamical motions. Conclusions and perspectives constitute the subject of Section VIII. Some technical details are relegated into an appendix.

II. MODEL AND SIMULATION METHOD

A. Amoeboid swimmer model

For simplicity, and due to a quite involved computational cost, we consider a 2D geometry. An amoeboid swimmer (AS) is modeled as a membrane and is immersed in a newtonian fluid domain of a given viscosity η . The encapsulated fluid is taken to have the same viscosity, for simplicity. We consider the pure Stokes regime (no inertia). An effective radius of the swimmer is defined as $R_0 = \sqrt{A_0/\pi}$, where A_0 is the enclosed area. We define an excess contour (excess counted from a circular shape) Γ as $\Gamma = L_0/(2\pi R_0) - 1$ to describe the degree of deflation of swimmer shape. $\Gamma = 0$ represents a circular shape, whereas a large enough Γ refers to a swimmer which can have ample shape deformations. The perimeter L_0 of the swimmer membrane is taken to be constant due to the inextensibility of the membrane. Extensible membranes can be dealt with as well, but our goal is to consider a minimal model in order to capture the basic features before refinement. The swimmer is confined between two rigid walls separated by a distance W . The fluid has a no-slip boundary condition on the walls. A schematic representation of the studied system with some useful notations are shown in Fig. 1.

We consider that the swimmer deploys certain forces from internal machinery (which are not the scope of the present paper, but in the section devoted to discussion we shall comment on this point), and those forces have a certain distribution at the membrane. These are called the active forces, denoted as \mathbf{F}_a , and they depend on the position of a material point of the membrane and on time (see below). The active forces have a natural tendency to expand (or compress) the membrane, so that the membrane will resist thanks to its intrinsic cohesive forces, resulting in a tension-like reaction. As we consider a purely incompressible membrane, the tension is such that the local arclength should remain constant in the course of time.

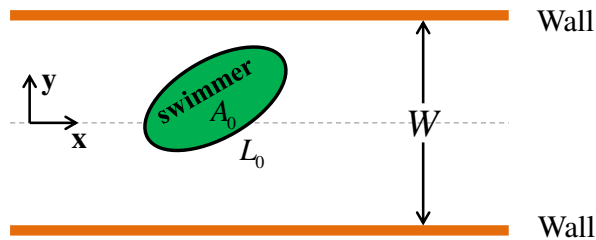


FIG. 1: (Color online) A schematic representation of the system and some useful notations. The swimmer has internal area A_0 and perimeter L_0 .

B. The choice of the active forces

The total force density (force per unit area) at the membrane is thus composed of an active part and a passive part, and can be written as

$$\mathbf{F} = F_a \mathbf{n} - \zeta c \mathbf{n} + \frac{\partial \zeta}{\partial s} \mathbf{t}, \quad (1)$$

where $F_a \mathbf{n}$ is the active force to be specified below and which we take to be directed along the normal direction, where \mathbf{n} is the unit normal vector. $\zeta(s, t)$ is a Lagrange multiplier that enforces local membrane inextensibility, c is the curvature, \mathbf{t} is the unit tangent vector, and s is the arclength. Because of the closed curve representing the swimmer, it is convenient to decompose the active force into Fourier series

$$F_a(\alpha, t) = \sum_{k=-k_{max}, |k| \neq 0, 1}^{k=k_{max}} \hat{F}_k(t) e^{ik\alpha}, \quad (2)$$

where we have defined the normalized arc length $\alpha = 2\pi s/L_0$. Actually, it turns out to be more efficient numerically to supplement the active force by an extra term $\mathbf{F}_0 + \tilde{F}_0 \mathbf{t}$, the first contribution is constant, and the second is purely tangential.

Our strategy is to keep the model as simple as possible, and therefore we will limit the expansion (2) to $k_{max} = 3$. The mode with $k = 0$ does not play a role since the fluid is incompressible ($k = 0$ corresponds to a homogeneous pressure jump across the membrane). For a swimmer having a shape close to a circle, the mode $k = 1$ corresponds to a translation mode, and is irrelevant. However, this ceases to be the case for shapes that deviate significantly from a circle. Still, to simplify the model we may take $F_1 = 0$. We are thus left with two complex amplitudes \hat{F}_2 and \hat{F}_3 . Again for simplicity, the imaginary parts of \hat{F}_2 and \hat{F}_3 are set to zero, so the active

force used in this work is taken to be [56]

$$F_a(\alpha, t) = 2F_2(t) \cos(2\alpha) + 2F_3(t) \cos(3\alpha). \quad (3)$$

F_2 and F_3 are time-dependent quantities expressing the fact that the cell executes some cyclic motion in order to move forwards. This cyclic motion should not be reversible in time, according to the Purcell theorem [34], owing to the reversibility of the Stokes equations upon time reversal. Following our first study on amoeboid motion [30] we shall make a simple choice for time dependence

$$F_2(t) = -A_2 \cos(\omega t), \quad F_3(t) = A_3 \sin(\omega t). \quad (4)$$

A_2 and A_3 are taken for simplicity to be equal ($A_2 = A_3 = A$). We are thus left with four parameters characterizing the force distribution, A , the scalar \tilde{F}_0 and the two components of \mathbf{F}_0 . We have to impose that the total force and the total torque are zero:

$$\oint \mathbf{F} ds = 0, \quad \oint \mathbf{r} \times \mathbf{F} ds = 0. \quad (5)$$

The integrals are performed over the swimmer perimeter. This leads to three equations in terms of x and y components that fix the three force components F_{0x} , F_{0y} and \tilde{F}_0 . We are thus left with a single parameter monitoring the force, namely the amplitude A .

Note that the total force and the total torque of our passive force related to ζ (eqn (1)) vanish automatically. Indeed, that part can be written as a functional derivative of an energy (see Ref. [35])

$$\mathbf{F}^{\text{mem}} = -\frac{\delta E(\mathbf{r}(s))}{\delta \mathbf{r}}, \quad (6)$$

where $\delta/\delta \mathbf{r}$ is the functional derivative. Since this energy is intrinsic to the membrane, any rigid translation or rotation leaves invariant the energy. Let $\delta \mathbf{r}$ be the displacement of a given point on the membrane during a time interval δt , corresponding to a rigid translation or rotation. In both cases the energy is unchanged and we have

$$\delta E(\mathbf{r}) = E(\mathbf{r} + \delta \mathbf{r}) - E(\mathbf{r}) = \oint [\mathbf{F}^{\text{mem}}(s) \cdot \delta \mathbf{r}(s)] ds = 0. \quad (7)$$

For a translation, $\delta \mathbf{r}$ is constant and is denoted as $\delta \mathbf{r}_0$, whereas for a rotation we have $\delta \mathbf{r} = \boldsymbol{\omega}_0 \delta t \times \mathbf{r} \equiv \delta \boldsymbol{\theta}_0 \times \mathbf{r}$, where $\boldsymbol{\omega}_0$ is the angular velocity. Applying condition (7) to both cases one obtains

$$\delta E(\mathbf{r}) = \begin{cases} \delta \mathbf{r}_0 \cdot \oint_{\partial \Omega} \mathbf{F}^{\text{mem}}(s) ds = 0 & (\delta \mathbf{r} = \delta \mathbf{r}_0), \\ \delta \boldsymbol{\theta}_0 \cdot \oint_{\partial \Omega} [\mathbf{r}(s) \times \mathbf{F}^{\text{mem}}(s)] ds = 0 & (\delta \mathbf{r} = \delta \boldsymbol{\theta}_0 \times \mathbf{r}). \end{cases} \quad (8)$$

An explicit proof of the fact that the passive forces do not contribute to the total force is given in Appendix.

C. Independent dimensionless parameters

To quantify confined amoeboid dynamics, we define a set of dimensionless parameters. The set of physical parameters are the swimmer area A_0 and perimeter L_0 (the area defines a length scale $R_0 = \sqrt{A_0/\pi}$), the channel width W , the viscosity of the fluid (taken to be the same outside and inside the swimmer) η , the shape relaxation (or adaptation) time $T_c = \eta/A$ due to active force application, and the stroke frequency $\omega = 2\pi/T_s$, where T_s is the stroke period. All together, we obtain a set of three dimensionless parameters (Γ was already introduced above, but is regrouped here with other dimensionless numbers for convenience of the reader)

$$\begin{cases} C = \frac{2R_0}{W}, \\ S = \frac{T_s}{2\pi T_c} = \frac{A}{\omega\eta}, \\ \Gamma = \frac{L_0}{2\pi R_0} - 1. \end{cases} \quad (9)$$

The first parameter defines the confinement strength, the second measures the ratio between the stroke period. A large S means that the stroke is so slow that the shape has ample time to adapt to the applied force, whereas a small S means that the stroke is so fast that the shape has not enough time to fully adapt to the applied force. Finally, recall that the third parameter is the excess length; a large Γ means a quite deflated swimmer.

III. NUMERICAL METHODS

We make use here of two methods: the boundary integral formulation [32] associated with the Stokes flow, and the immersed boundary method [33], which incorporates inertial effects, as well as arbitrary shape of the boundaries and their compliance, for future studies. We shall briefly recall below the two methods.

A. Boundary integral method with two parallel plane walls

The general discussion of the BIM can be found in [36] and application to the present problem in [32]. Due to the linearity of the Stokes equations we can convert the bulk equations into a boundary integral equation which relates the velocity on the membrane to the forces exerted on the membrane

$$\mathbf{u}(\mathbf{r}_m, t) = \frac{1}{4\pi\eta} \oint \mathbf{G}(\mathbf{r}'_m, \mathbf{r}_m) \mathbf{F}(\mathbf{r}'_m, t) ds(\mathbf{r}'_m), \quad (10)$$

where the integral is performed over the membrane, with \mathbf{r}_m the membrane instantaneous position, $\mathbf{u}(\mathbf{r}_m, t)$ is the instantaneous velocity of a membrane point, \mathbf{F} is the total force from the membrane (eqn (1)). The unknown Lagrange multiplier ζ entering the total force (eqn (1)) is determined by requiring the divergence of velocity field along the membrane to be zero (membrane incompressibility condition). $\mathbf{G}(\mathbf{r}'_m, \mathbf{r}_m)$ is the Green's function which vanishes at the bounding walls (i.e. at $y = \pm W/2$) [32]. In an unbounded domain the Green's function is nothing but the Oseen tensor, which reads in 2D

$$G_{ij}(\mathbf{x}, \mathbf{y}) = -\delta_{ij} \ln r + \frac{r_i r_j}{r^2}, \quad (11)$$

where $r_i = x_i - y_i$ and $r^2 = r_i^2$ (Einstein convention is adopted). However, this function does not vanish at the wall. Therefore two alternatives are possible: (i) either use this function, and in which case we have to add to (10) an extra integral term (the integrand contains the product of the Green function and the hydrodynamic force on the boundaries), see Ref. [37], or (ii) find a Green function that vanishes at the walls. No explicit Green's function vanishing at the walls is available, but can be expressed in terms of a Fourier integral [32]. The advantage of the latter alternative is the absence of integral terms on the walls (the integral is performed on the swimmer membrane only), and that therefore the system size along the wall (x direction) can be taken as infinite, thus avoiding any potential numerical problem (like dependence of the results on system size) related to boundary condition along x . Some of the technical details of how the problem is numerically solved can be found in Ref. [32].

B. Immersed boundary method

We present now the other method which can allow, in principle, to have arbitrary bounding geometry as well as deformable walls, a work which is planned in the future. Therefore, it is essential to compare the two methods in this paper, before exploring the versatility of this method. The immersed boundary formulation is an Eulerian-Lagrangian framework in which fluid variables are defined in Eulerian manner, while the membrane related variables are defined in Lagrangian manner. The swimmer membrane as a moving inextensible interface, immersed in a 2D fluid domain Ω , is represented in a Lagrangian parametric form as $\mathbf{R}(\alpha, t) = (X(\alpha, t), Y(\alpha, t))$, where $\alpha \in [0, 2\pi]$ is a parameter of the initial configuration of the membrane. Thus, the governing equations of the Navier-Stokes fluid system are

$$\left\{ \begin{array}{ll} \rho \left(\frac{\partial \mathbf{u}}{\partial t} + (\mathbf{u} \cdot \nabla) \mathbf{u} \right) = -\nabla p + \eta \Delta \mathbf{u} + \int_0^{2\pi} \mathbf{F}(\alpha, t) \delta(\mathbf{r} - \mathbf{R}(\alpha, t)) |\mathbf{R}_\alpha| d\alpha & \text{in } \Omega, \\ \nabla \cdot \mathbf{u} = 0 & \text{in } \Omega, \\ \frac{\partial \mathbf{X}(\alpha, t)}{\partial t} = \mathbf{U}(\alpha, t) = \int \mathbf{u}(\mathbf{r}, t) \delta(\mathbf{r} - \mathbf{R}(\alpha, t)) d\mathbf{r} & \text{on } \partial\Omega. \end{array} \right. \quad (12)$$

where ρ represents the mass density, and the Eulerian fluid and Lagrangian immersed variables are linked by the 2D Dirac delta function $\delta(\mathbf{r}) = \delta(x)\delta(y)$. The total membrane force \mathbf{F} consists of the same active force as in BIM and the tension force $\mathbf{F}_\xi = \frac{1}{|\mathbf{R}_\alpha|} \xi_\alpha \mathbf{t} - \xi \mathbf{c}\mathbf{n}$ (the subscript α designates derivative), where ξ is a Lagrange multiplier that enforces the membrane inextensibility. We adopt the spring-like elastic force to approximate the membrane inextensibility, that is, taking $\xi = \xi_0(|\mathbf{R}_\alpha| - |\mathbf{R}_\alpha|^0)$ with a large stiffness constant ξ_0 , where $|\mathbf{R}_\alpha|^0$ is the local stretching factor of the membrane initial configuration [31, 33]. Details of numerical procedure can be found in references [31, 33].

We perform the time-stepping scheme as follows: The governing equations are discretized by the IBM. We consider the computational domain as a rectangle $\Omega = [a, b] \times [c, d]$; the no-slip boundary condition for the velocity is imposed on the two walls $y = c, d$ and no-flux condition is applied on $x = a, b$ for each fluid variables. Within this domain, a uniform Cartesian grid with mesh width h in both \mathbf{x} and \mathbf{y} directions is employed. The fluid variables are defined on the standard staggered marker-and-cell (MAC) manner [38]. That is, the velocity component u and v are defined at the cell-normal edges $(x_{i-1/2}, y_j) = (a + (i-1)h, c + (j-1/2)h)$ and $(x_i, y_{j-1/2}) = (a + (i-1/2)h, c + (j-1)h)$ respectively, while the pressure p is defined at the cell center $(x_i, y_j) = (a + (i-1/2)h, c + (j-1/2)h)$. For the membrane interface, we use $\alpha_k = k\Delta\alpha, k = 0, 1, \dots, M$ with $\Delta\alpha = 2\pi/M$ to represent the Lagrangian markers $\mathbf{R}_k = \mathbf{R}(s_k)$ so that any spatial derivatives can be performed spectrally accurate by using Fast Fourier Transform (FFT) [39]. Detailed numerical algorithm can be found in a previous work [33].

IV. AXIALLY MOVING SWIMMER

We first consider an amoeboid swimmer (AS) initially located in the center of the channel, that is, its initial center of mass is $(X_c, Y_c) = (0, 0)$. Although this axial motion is generically found to be an unstable solution (see Section VII), it gives useful insights into the dynamics of the confined amoeboid swimmer. Figure 2 shows a typical snapshot over 170 deformation cycles. For quite a long period of time (in our simulation this solution survives for few hundreds of cycles), the swimmer moves along the channel (x direction).

Figure 3 shows the center of mass of the swimmer, $X_c(t)$, undergoes a periodic oscillation in the axial direc-

tion as shown in (a). A first observation is that for C not too large (from $C = 0.01$ up to $C = 0.71$), the amplitude of the oscillation increases with confinement. The slope of the curves $X(t)$ also increases with C indicating an enhancement of migration speed upon increasing confinement. The increase of the amplitude deformation with C (for not too large C) is already an interesting indication that the swimmer takes benefit of the walls to enhance its migration speed.

In physical units the average velocity of the swimmer will be defined as $\langle V \rangle = (X_c(t+T_s) - X_c(t))/T_s$ (which is the net displacement of the center of mass over one cycle divided by the stroke cycle period). We will define a dimensionless instantaneous velocity as $\bar{V} = VT_s/R_0$. Its average over one swimming cycle is defined as $\langle \bar{V} \rangle = \bar{X}_c(t+T_s) - \bar{X}_c(t)$, where $\bar{X}_c = X_c/R_0$. Fig. 3 (b) shows that the instantaneous velocity changes during three deformation stroke periods. The negative velocity is induced by the confined walls, since in the unconfined case the velocity remains always positive [30].

A. Scaling of the swimming velocity with the force amplitude

Due to the linearity of the Stokes equations, it may be expected that the velocity of the swimmer is linear with the force. Note also that for the various swimmers modeled as rigid body studied so far, like *E. coli* [5, 6], *Bacillus subtilis* [7] (examples of the so-called pushers), *Chlamydomonas* (an example of puller) [4, 8, 9], the migration speed is taken in models as a linear function of the force amplitude. In contrast, we find that the AS

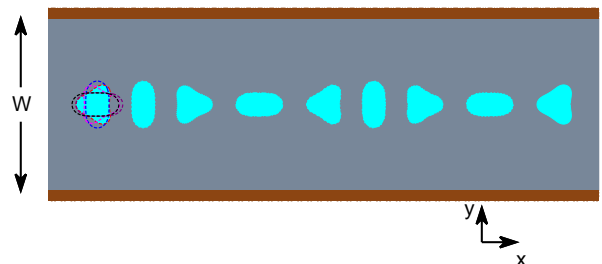


FIG. 2: (Color online) Snapshots of an axially moving swimmer over time ($W = 10.0R_0$). The dashed profiles show a complete period T_s of deformation and then a few shapes are represented over a time of the order of $170T_s$. $\Gamma = 0.085$, $S = 10$.

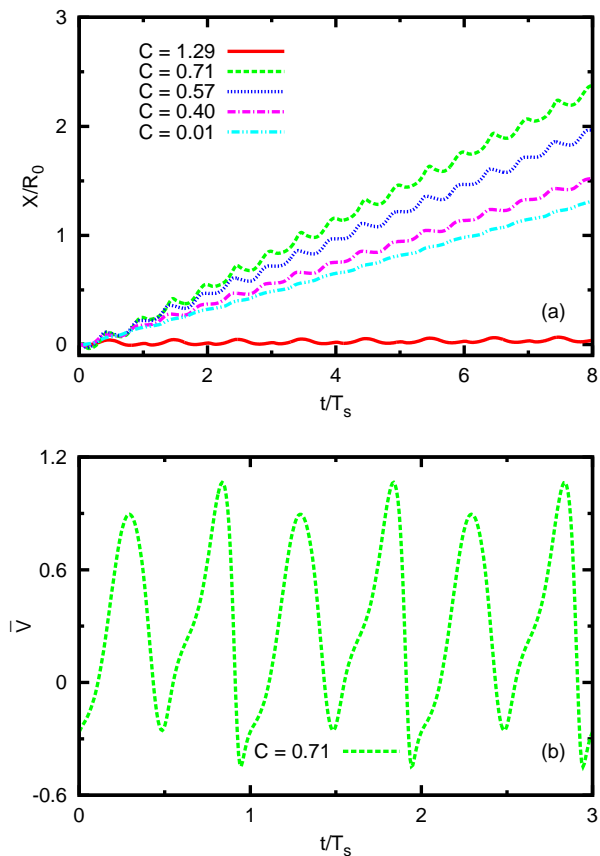


FIG. 3: (Color online) (a) An axially moving amoeboid swimmer undergoes a periodic oscillation in the axial direction (X direction) of the channel as a function of time. From strong to weak confinements, the corresponding oscillation motions are represented by different types of colorful lines. (b) Velocity of an axially moving swimmer as a function of time. $\Gamma = 0.085$, $S = 10$.

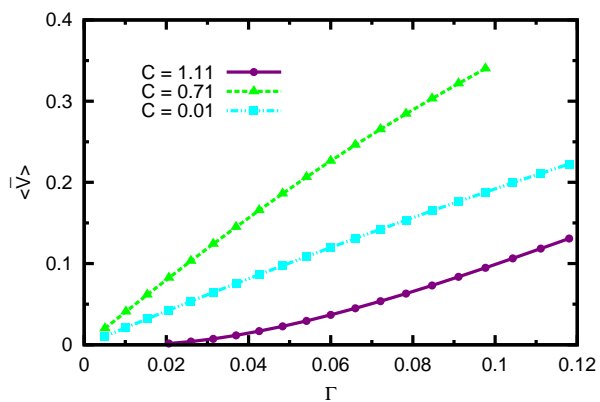


FIG. 4: (Color online) In different confined regions, the linear and nonlinear relations between the excess length Γ and the velocity magnitude \bar{V} are calculated. The fitting exponent for the weak confinement ($C = 0.01$) is almost 1, for the intermediate confinement ($C = 0.71$) is less than 1, while it is larger than 1 for the strong confinement ($C = 1.11$). $S = 10$.

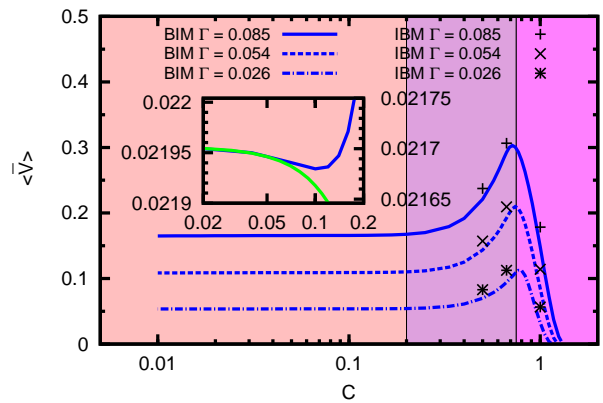


FIG. 5: (Color online) Time-averaged velocity magnitudes as a function of C in log scale for different Γ 's. The data represented by the solid lines are calculated by BIM, while the data represented by symbols are calculated by IBM. $S = 10$. The inset shows a zoom for weak confinement with $\Gamma = 0.010$ showing a weakly decreasing velocity (scale on the left side) and its comparison with the analytical theory (presented at the end of section V), with the scale on the right side. The full numerical analysis and the analytical one agree quite well as long as the confinement is weak enough, which is the assumption of the analytical work.

markedly differs from the above swimmers category. The velocity is found to be a nonlinear function of the force amplitude. Recall that the force amplitude is denoted as A . We have defined in eqn (9) a set of three dimensionless parameters. Since our goal in this section is to discuss the effect of the force amplitude, we set Γ and C to constant values. The physical (i.e. not the dimensionless) average velocity over a swimming cycle is given, from dimensional analysis, by the relation

$$\langle V \rangle \sim \frac{R_0}{T_s} G(S). \quad (13)$$

where $G(S)$ is a scaling function, which is unknown for the moment. Let us first provide some supports to the behavior of $G(S)$ based on physical intuition. An obvious guess is that for a large S , $\langle V \rangle$ should be independent of the force amplitude. Indeed, recall that S can be written as $S \sim T_s/T_c$. This is the ratio between the stroke period and the shape adaptation time (that is the time needed for the swimmer to adapt to the applied forces). A large S (meaning also large enough force amplitude) implies that the swimmer attains its saturated shape (in response to applied forces) in a shorter time than the stroke time interval. In other words, increasing further the force amplitude will just result in a faster shape adaptation before the stroke cycle can be duplicated. This increase of A does not promote a faster swimming, but just a faster adaptation time. Indeed, in the Stokes regime time does not matter but only the configuration does. Therefore, the speed should attain a plateau at large S . Our numerical simulation clearly shows this behavior (Fig. 6).

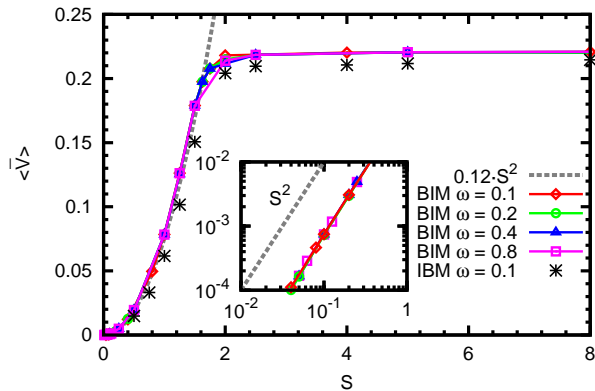


FIG. 6: (Color online) (a) The time-averaged velocity magnitude attains a plateau with increasing the dimensionless amplitude of active forces S ; $\Gamma = 0.085$ and $C = 0.5$. The inset shows the scaling S^2 (grey dashed line) in a log – log plot. The stars are data obtained by IBM, the other data are obtained by BIM.

We can thus conclude that for large S , $\langle V \rangle \sim \omega R_0$. The velocity is thus fixed only by the stroke frequency.

The situation is less obvious for small S . This limit means that the force configuration changes in time faster than the shape adaptation occurs. Increasing S (but still in the small range limit), means the shape has more time to adapt (but not yet fully adapt), resulting in a faster and faster motion, since the shape will, for each increase of S , be deployed more and more until saturation (when the force is large enough). The first natural expectation would have been a linear relationship between velocity and force. This naive expectation does not comply with the numerical finding. Our results show a quadratic behavior. A qualitative argument in favor of this behavior is the following. The velocity is a priori, to leading order, proportional to A . However, the motion is possible only if the swimmer deforms, a deformation which is also proportional to A , to leading order, hence a quadratic behavior of $\langle V \rangle$ with A .

In summary, the velocity of the swimmer behaves as

$$\langle V \rangle \sim \begin{cases} (R_0/T_s)S^2 = R_0T_sA^2/\eta^2 & (S \ll 1), \\ R_0/T_s & (S \gg 1). \end{cases} \quad (14)$$

Figure 6 shows the full nonlinear behavior obtained from the numerical solution which is in agreement with the above scalings. Note that the velocity behaves, at small force, as $1/\eta^2$, which is distinct from the classical Stokes result where the velocity is $\sim 1/\eta$. This behavior is not devoid of experimental testability (provided that the swimmer operates at a fixed given force when viscosity is varied). It is not however clear if the condition of $S \ll 1$ is abundant or not in the amoeboid swimming world. It is also of great importance to conceive of artificial amoeboid swimmers that can be monitored in order to scan the whole range of S where the scaling relations presented above can be tested.

B. Velocity of the swimmer as a function of confinement and excess length

We have determined the velocity as a function of the deflation of the swimmer, a deflation characterized by the excess length Γ . Quasi-linear and nonlinear relations between the velocity magnitude \bar{V} of the center of mass and the excess length Γ are found depending on confinement, as shown in Fig. 4. We expect that the more the swimmer is deflated the larger is its velocity. Indeed, the amplitude of deformation of the swimmer increases with Γ , which thus implies a higher speed. From Fig. 4, it is found that the exponent for the weak confinement is almost 1 (shown by a purple line in Fig. 4), and agrees with the study for a completely unbounded swimmer [30]. However, the confinement provides a complex picture: we have a superlinear behavior in the intermediate confinement regime (shown by a cyan dotted line in Fig. 4), while it is sublinear for the strong confinement case (shown by a green line in Fig. 4). A prominent property we have recently reported on [31] is the fact the velocity has a non monotonous behavior with confinement C . The results are summarized in Fig. 5, where we compare the outcome of the two numerical methods, which show a quite good agreement, and both show a maximum in the $\langle \bar{V}(C) \rangle$ curve.

Given the tendencies of the evolution of velocity in Fig. 5, it is tempting to classify the confinement into three distinct regions (color from light to dark corresponds to C varying from weak to strong): the weak confinement $C \leq 0.2$ (pink zone), the intermediate confinement $0.2 < C < 0.7 \sim 0.8$ (depending on Γ , plum zone), and the strong confinement $C \geq 0.7 \sim 0.8$ (depending on Γ , orchid zone). This classification is dictated by the fact that $\langle \bar{V} \rangle$ remains almost constant in the weak confinement regime, then quickly increases in the intermediate confinement, while abruptly drops down in the strong confinement regime.

V. ON THE NON MONOTONOUS BEHAVIOR OF THE SWIMMER VELOCITY AS A FUNCTION OF C

Once we have clarified the role of the force amplitude in the swimming speed, we would like to discuss the behavior of the velocity as a function of the confinement (Fig. 5). We will first provide a brief summary on the wall effects reported so far in the literature before discussing our results. The fact that the wall enhances motility is reported in several papers [11, 40–45]. However, we must stress, as we found, that this is not a systematic tendency. A close inspection shows that at weak confinement the velocity may also exhibit first a decreasing (before increasing) behavior; see below.

Felderhof [40] has shown that the speed of Taylor-like swimmer increases with confinement. In contrast, Zhu *et al.* [41] used the squirmer model to show that (when

only tangential surface motion are included) the velocity *decreases* with confinement. When including normal deformation they found an increase of velocity with confinement. Liu *et al.* [45] analyzed a helical flagellum in tube and found that, except for a small range of tube radii, the swimming speed, when helix rotation rate is fixed, increases monotonically as the confinement becomes tighter. Acemoglu *et al.* [44] adopted a similar model but, besides the flagellum, they included a head and found a contrasted result, in that a *decrease* of velocity with confinement. Bilbao *et al.* [42] treated numerically a model inspired by nematode locomotion and found that it moves faster due to walls. Ledesma *et al.* [43] reported on a dipolar swimmer in a rigid and an elastic tube and found a speed enhancement due to walls.

A. The flow field

In this section we would like to provide some qualitative picture regarding the increase of swimming velocity when the confinement increases. At first sight, one qualitative argument is that the swimmer grasps on the wall in order to enhance its motion. When the confinement is too large, the swimmer can not fully deploy its shape and therefore a collapse of the velocity is expected. Actually the situation is more subtle as will be discussed below.

Let us analyze in some details the flow pattern around the swimmer as well as the dissipation, which provide some hint towards understanding the basic mechanisms. We shall then point out some analytical results that show the complex nature of the phenomenon. Fig. 7 shows the flow pattern around the swimmer. It consists of two swirlings which lie inside the AS. We also see there the "grasping" nature of the flow field on the walls. The flow pattern has a source dipole like structure. A source in 2D creates a flow which is inversely proportional to distance in 2D, meaning that the source dipole has an asymptotic behavior which is inversely proportional to the distance to the square.

B. Dissipation function

An instantaneous intensity of dissipation density can be calculated as the rate of the work performed by the viscous force as follows:

$$\Psi_v = \sigma_{ij} \frac{\partial u_i}{\partial x_j} = 2\eta \epsilon_{ij} \epsilon_{ij}, \quad (15)$$

where $\sigma_{ij} = -p\delta_{ij} + 2\eta\epsilon_{ij}$, $\epsilon_{ij} = 1/2(\partial_j u_i + \partial_i u_j)$, and repeated subscripts are to be summed over. The expression reads explicitly in $x - y$ coordinates as

$$\Psi_v = 2\eta \left[\left(\frac{\partial u_x}{\partial x} \right)^2 + \left(\frac{\partial u_y}{\partial y} \right)^2 \right] + \eta \left(\frac{\partial u_x}{\partial y} + \frac{\partial u_y}{\partial x} \right)^2 \quad (16)$$

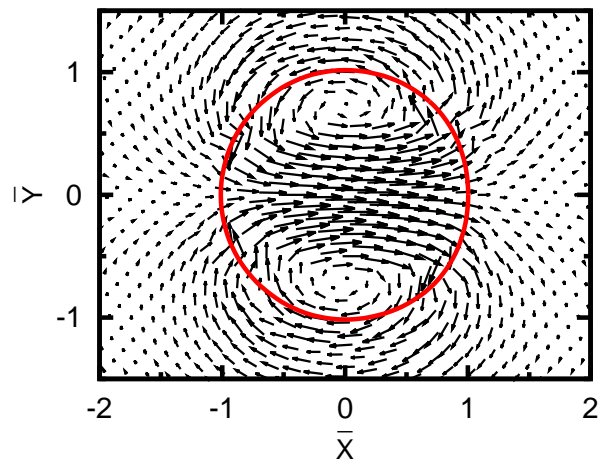


FIG. 7: (Color online) The time-averaged shape of the swimmer over one swimming cycle and its corresponding velocity field. $C = 0.40$, $\Gamma = 0.085$, $S = 10$.

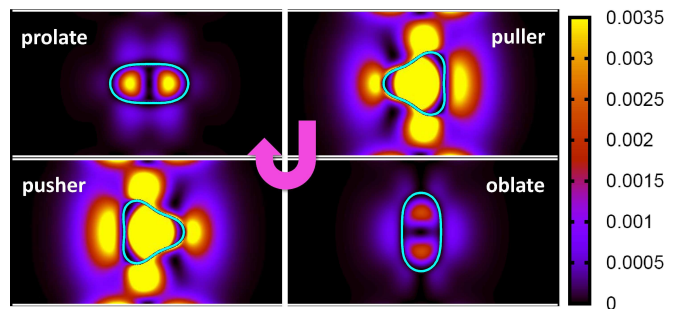


FIG. 8: (Color online) A series of instantaneous dissipation distributions corresponding to instantaneous shape deformation during one complete swimming stroke. Color shows the intensity of dissipation density, and blue color represents the contour of swimmer. Swimming direction points to the right side. An amoeboid swimmer combines pusher and puller nature during one deformation period. $C = 0.40$, $\Gamma = 0.085$, $S = 10$.

The rate of work (output power) performed by AS is instantaneously (actually only the active forces perform work but not the tension part) equal to the rate of total energy dissipation in the fluid. The hydrodynamic interactions between the swimmer and the walls are illustrated by a series of instantaneous dissipation patterns produced during the process of one complete AS stroke in Fig. 8. The corresponding instantaneous configurations of a wall-confined amoeboid swimmer are plotted by a closed cyan solid line (see Fig. 8), from which we can clearly observe that the swimmer uses the wall as a support on which much of the work is performed (grasping). The instantaneous dissipation shows two arm-like distribution extended to double walls during the instantaneous puller and pusher states [30], so that one can intuitively understand that the swimmer's speed is increased by extended arm-like dissipation structures by hydrodynamically

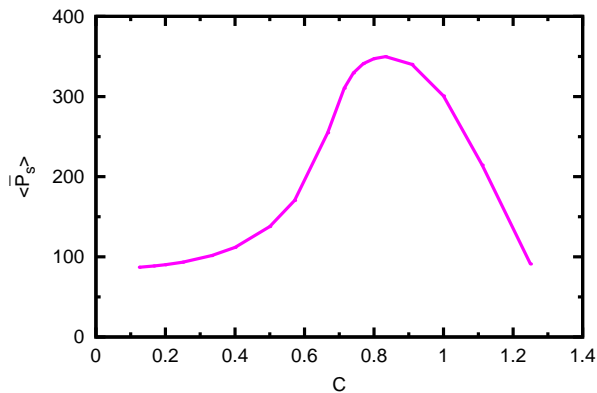


FIG. 9: (Color online) The time-averaged power consumption $\langle \bar{P}_s \rangle$ as a function of C for $\Gamma = 0.085$, $S = 10$.

cal friction with the walls. Movies on the instantaneous dissipation pattern changing during the swimming cycle are available from supp. material [46].

We define a time-averaged power consumption (rate of work) as

$$\begin{aligned} \langle P_s \rangle &= \frac{1}{T_s} \int_0^{T_s} \oint_{\partial\Omega} [\mathbf{F}(s) \cdot \mathbf{u}(s)] ds dt \\ &= \langle \oint_{\partial\Omega} [\mathbf{F}(s) \cdot \mathbf{u}(s)] ds \rangle, \end{aligned} \quad (17)$$

where T_s is a swimming period. A dimensionless average power is defined as $\langle \bar{P}_s \rangle = \langle P_s \rangle T_s^2 / (\eta R_0^2)$. Fig. 9 shows the dimensionless time-averaged power of the active forces. Power consumption $\langle \bar{P}_s \rangle$ attains a maximum at a confinement which is close (but not equal) to the confinement at which a maximum velocity is obtained (Fig. 5). In the strongly confined regime, the power rapidly decreases due to the fact that the deformation amplitude is strongly reduced due to the walls constraint: the swimmer is in principle able to deploy a larger amplitude but the rigid walls act against this tendency. This picture is supported by a recent experiment [47] according to which the flagellar wave amplitude of bull sperm in the extremely confined condition is so strongly suppressed that they have to adopt a slither way to swim along a rigid surface. The swimming velocity of bull sperm becomes slower and slower.

Note finally that an analytical study, on which we will report in great details elsewhere [48], performed at weak confinement has allowed us to extract the swimming velocity as a function of confinement:

$$\langle \bar{V} \rangle = \frac{5\pi\Gamma R_0}{3\sqrt{6}T_s} - 0.12C^2 \frac{\pi\Gamma R_0}{T_s} + O(C^3\Gamma) + O(\Gamma^{3/2}). \quad (18)$$

The first term corresponds to the purely unconfined case and we capture the same dependence with Γ as in the 3D case [30]. The second term is the first contribution of confinement to the swimming speed, and is negative,

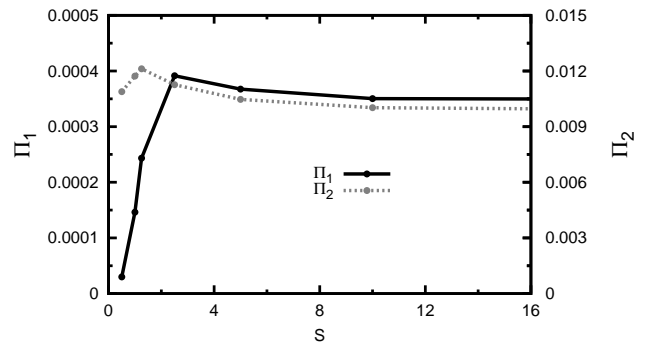


FIG. 10: (Color online) The two efficiencies Π_1 and Π_2 as functions of S . $C = 0.5$ and $\Gamma = 0.085$.

meaning that at very small confinement the wall reduces the swimming speed. This is visible in inset of Fig. 5. This remark shows clearly that the effect of the walls is not quite obvious.

VI. EFFICIENCY OF SWIMMING

In this section we wish to investigate the notion of efficiency. We will first adopt a widely used definition of swimming efficiency, which is the ratio of the least power required to drag (or pull) the swimmer along the axis at its time-averaged speed $\langle V \rangle$ (the physical one, not the dimensionless one) over the actual time-averaged output power $\langle P_s \rangle$ generated by the swimmer [49–51]. Here we define a dimensionless 2D efficiency Π_1 as

$$\Pi_1 = \frac{\eta \langle V \rangle^2}{\langle P_s \rangle}, \quad (19)$$

where $\langle V \rangle$ is the average physical velocity. Figure 10 shows that the optimal swimming occurs at the transition point where the velocity as a function of the applied force saturates (see Fig.6). The qualitative behavior of the efficiency curve can be explained as follows. When S is small (small force, before the plateau is reached in Fig.6) the stroke dynamics is so fast that it does not allow to the swimmer to attain its saturated shape, and the swimmer loses efficiency. If S is too large, this does not bring any benefit since the swimmer reaches too fast its saturated shape, and does not gain in efficiency if the force is increased further.

It is also worthwhile to examine the efficiency as a function of the strength of confinement C . Following the definition above, we find that the maximum efficiency occurs at a confinement of $C \simeq 0.6$, which is different from that corresponding to the maximum speed (Fig. 5, $C \simeq 0.75$). The efficiency Π_1 first gradually increases and then decreases rapidly after the optimal point.

A second swimming efficiency which has been considered in literature is noteworthy. It is defined as $\sim \langle V \rangle / \langle P_s \rangle$ [52, 53] and seemed to be suitable for small

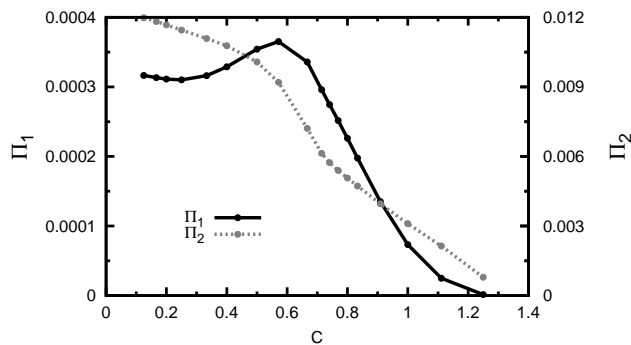


FIG. 11: The efficiencies Π_1 and Π_2 as functions of C for $\Gamma = 0.085$, $S = 10$.

deformations. Since for small deformation, $V \sim \Gamma$, then $P_s \sim \Gamma$, the efficiency is independent of Γ . This definition of efficiency is not dimensionless. We adopt here a dimensionless form given by

$$\Pi_2 = \frac{\eta\omega R_0 \langle V \rangle}{\langle P_s \rangle}. \quad (20)$$

The corresponding results are shown by the grey dashed dotted line in Fig. 9 and Fig. 11, from which no optimal value for a special confinement is found, in contrast to the definition (19). This example clearly highlights the main difference between the two definitions. It also points to the fact that there seems to be no straightforward definition of a suitable efficiency (if any).

VII. VARIOUS DYNAMICAL STATES OF THE SWIMMER: FROM STRAIGHT TRAJECTORY TO NAVIGATION

In this section we present the rich panel of behaviors manifested by the AS. We shall see that the AS can settle into a straight trajectory, or can navigate in the channel with a fixed amplitude in a symmetric or asymmetric way, or can also crash into the wall. The adoption of one regime or another depends on various conditions, and especially on the force distribution and on the degree of confinement. One extra degree of complexity that is unique to the AS is the fact the nature of the swimmer (puller or pusher) is not an intrinsic property of the swimmer itself, but depends on the environment (say on confinement). Before discussing our results, we would like first to put our work in the context of swimmers in general.

Zhu *et al.* [41] adopted the squirmer model which can be set to be a pusher, a puller or neutral, thanks to an appropriate choice of parameters. They find that a pusher crashes into the wall, a puller settles into a straight trajectory, and a neutral swimmer navigates. However, the navigation amplitude depends on initial conditions, in that it is not a limit cycle, but an oscillator, which is akin to what happens for Hamiltonian systems.

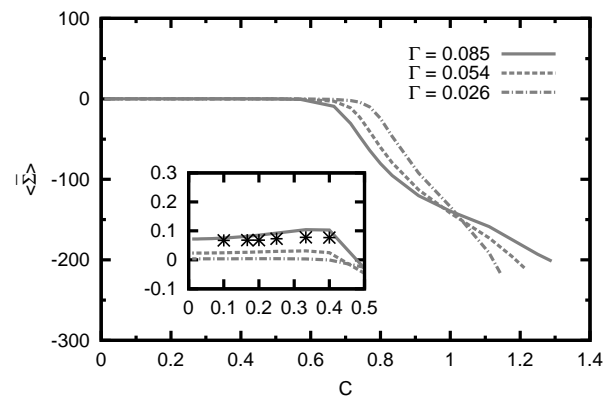


FIG. 12: (Color online) Time-averaged stresslet $\langle \bar{\Sigma} \rangle$ as a function of confinement C showing the transition from pusher to puller. Different lines refer to an axially moving swimmer and stars to a symmetrically navigating swimmer. Inset shows a zoom for small C in order to show the confinement at which the pusher-puller transition occurs. $S = 10$.

Najafi *et al.* [54] used a three-bead model and reported on the possibility for the swimmer to navigate. It was not clear if the navigation amplitude depends or not on initial conditions. Since the nature of the swimmer seems to play an important role, it is interesting to define first in our system the nature of the swimmer before presenting the main results.

A. Swimmer nature evolution

In the far-field approximation, the first contribution (in a multipolar expansion) to the velocity field is governed by a term of the form $\Sigma_{ij} = \oint F_i r_j ds$. Exploiting symmetry of the swimmer (axial symmetry) we can write that the far field is, to leading order, proportional to $\bar{\Sigma} = (\Sigma_{xx} - \Sigma_{yy})/(\eta R_0^2/T_s)$, which we will call (dimensionless) stresslet hereafter. The instantaneous type (pusher or puller) of an AS can be judged by the sign of the instantaneous stresslet: ($\bar{\Sigma} > 0$ indicates a pusher and $\bar{\Sigma} < 0$ indicates a puller). As already pointed earlier [30] our swimmer can have during time a complex nature which consists of an entangled puller-pusher state. We could split the swimming cycles into 4 intervals. In a given time interval of the swimming cycle the swimmer behaves as a pusher, followed by an interval where it behaves as a mixed pusher-puller state, then in a third interval it behaves as a puller, and then as a mixed state (see also Fig.8). One possible way of characterizing our swimmer is to determine its nature on average over one swimming cycle. The dimensionless average stresslet is given by $\langle \bar{\Sigma} \rangle = (\int_0^{T_s} \bar{\Sigma} dt)/T_s$ (average over one deformation period T_s). Figure 12 shows this quantity as a function of confinement. The swimmer behaves as a pusher for $C \lesssim 0.5$, while as a puller for $C > 0.5$. The efficiency shown in Fig. 11 shows an optimum for $C \sim 0.6$ which

is close to the pusher-puller transition. Whether this is accidental or reflects some general facts, is at present not understood. In the next section we analyze this quantity and link it with the nature of the swimmer motion. Note that when the swimmer trajectory corresponds to a symmetric navigation the far field over a navigation period is also proportional to $\langle \bar{\Sigma} \rangle$.

B. Navigation and symmetry-breaking bifurcation

An outstanding feature of the AS is that its nature (puller or pusher) is not an intrinsic property. More precisely, this nature can change with confinement. By using the force distribution presented in Section II B we have analyzed the nature of the swimmer. We find that the swimmer behaves as a pusher for a weak confinement, while it behaves as a puller at a stronger confinement. The results are shown in Fig. 12. In the weak confinement regime (where the swimmer is a pusher on average) it is found that the straight trajectory is unstable against navigation, and that the navigation amplitude is a function of confinement and is independent of initial conditions. This is confirmed by both numerical methods (BIM and IBM). Snapshots of the navigation are shown in Fig. 13 where one can observe ample navigation of the swimmer. Typical evolution of the Y position as a function of time is shown in Fig. 14. This curve shows a small scale structure associated with the strokes of the swimmers and a large scale navigation period. Figure 15 displays some trajectories (Y as a function of X) of the navigating mode showing a quite complex structure. Let us define the navigation amplitude ΔY as the difference between the maximum of $Y(t)$, Y_t , and the minimum of $Y(t)$, Y_b , $\Delta Y = Y_t - Y_b$ and plot this amplitude as a function of confinement C (Fig. 16). We see that the amplitude decreases with C . The swimmer does not crash into the wall, in contrast with the squirmer model studied in Ref. [41]. Indeed, we find that the amplitude of navigation stays finite in the course of time. The navigation mode survives also when the swimmer behaves as a puller on average, and does not settle into a straight trajectory. In Fig. 16 the domains of puller and pusher are shown.

The navigation mode undergoes an instability at a critical confinement $C \simeq 0.8$ (where it behaves as a puller) in favor of an asymmetric motion where the swimmer moves closer to one of the two walls. The amplitude $Y(t)$ of the center of mass is shown in Fig. 17. The center of mass shows an oscillation which is fixed by the stroke frequency, in contrast to the navigating mode which, apart from small scale oscillation due to the strokes, develops large scale oscillations of the position. Figure 18 shows the trajectory of the asymmetric swimmer. The overall behavior is summarized in Fig. 19. There we show the average position of the center of mass as a function of confinement C . For small C , the center of mass position averaged over a navigation period is zero. The swimmer

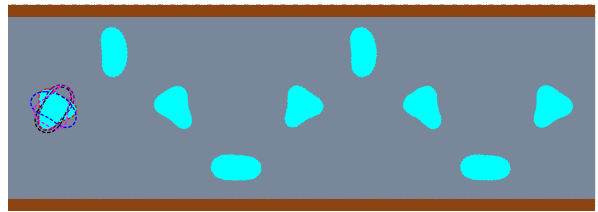


FIG. 13: (Color online) Snapshots of a navigating swimmer over time ($W = 10.0R_0$). The dashed profiles show a complete period T_s of deformation. Few shapes are represented over two navigation periods T of the order of $240T_s$. $\Gamma = 0.085$, $S = 10$.

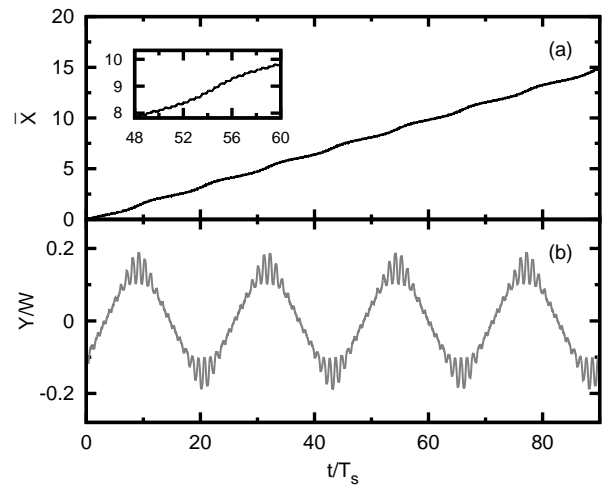


FIG. 14: (Color online) A navigating amoeboid swimmer in the channel undergoes periodic oscillations in both x (a) and y (b) directions. The inset in (a) shows the short periodic oscillations due to strokes which are superimposed on the long periodic oscillations due to the navigation. $C = 0.50$, $\Gamma = 0.085$, $S = 10$.

undergoes a spontaneous symmetry-breaking bifurcation at $C \sim 0.8$ where it moves towards either of the two walls. In this regime the swimmer center of mass shows temporal oscillations which are symmetric (lower rectangle in the figure). The bifurcation is supercritical (albeit quite abrupt). At a certain confinement $C = 1.04$, the average position of the center mass changes sign.

C. Ability of scanning space

An interesting question is to analyze the ability of the swimmer for scanning the offered space. We measured the highest membrane point of the swimmer in the channel and call it H_t and the lowest membrane point, and call it H_b . The difference $\Delta H = H_t - H_b$ is a direct measure of space scanning by the swimmer. In Fig. 21 (top panel) we provide a schematic representation of this measure. The lower panel provides the numerically com-

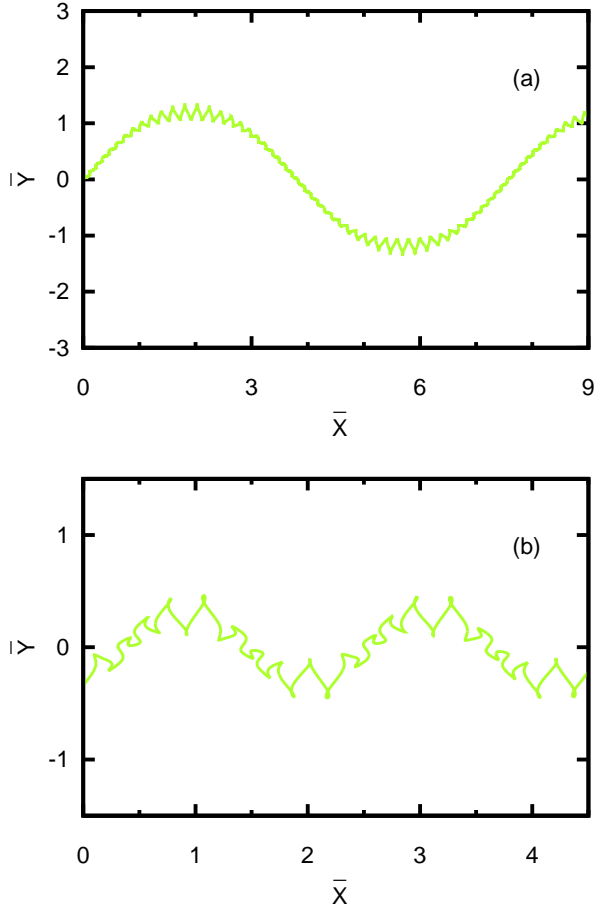


FIG. 15: (Color online) Trajectories of the center of mass ($\Gamma = 0.085$) for three different values of the strength of confinement. (a) $C = 1/3$, (b) $C = 2/3$. Navigation is symmetric. $S = 10$.

puted scanning amplitude as a function of confinement. It is found that the navigating mode can explore between about 80% and 95% of the available lateral space.

D. Crashing into the wall and settling into a straight trajectory

As stated above it has been reported [41] (by adopting a squirmer model) that the pusher crashes into the wall while a puller settles into a straight trajectory. This contrasts with our finding presented above. We have thus attempted to investigate this question further in order to clarify the situation. We find that the type of trajectory depends strongly on the strength of the stresslet $\bar{\Sigma}$ and the strength of a linear combination \bar{D} of dimensionless force quadrupole $\bar{\Sigma}_2$ and source dipole $\bar{\Delta}_2$ [31]. A weak pusher or puller means that the stresslet $\bar{\Sigma}^2 < \bar{V}\bar{D}$ [31], where \bar{D} is the dimensionless force quadrupole strength. For example, if the swimmer is a weak pusher, we have navigation and symmetry-breaking as presented above. On the contrary, if the pusher is strong enough we also

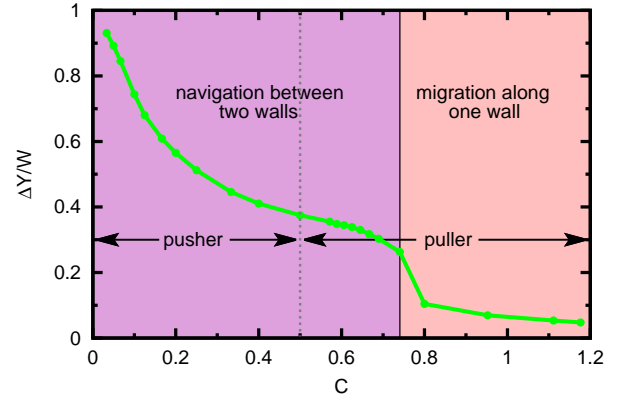


FIG. 16: (Color online) The amplitude of navigation as a function of confinement C . $\Gamma = 0.085$, $S = 10$.

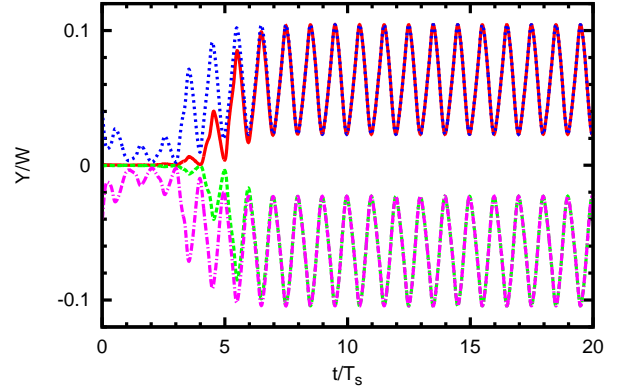


FIG. 17: (Color online) The vertical position of center of mass Y as a function of time t showing the symmetry breaking bifurcation. Different colors represent different initial positions. $\Gamma = 0.085$, $S = 10$, $C = 0.8$.

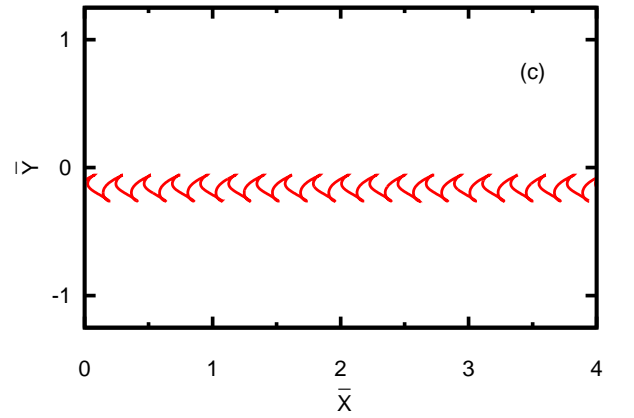


FIG. 18: (Color online) A trajectory of the asymmetric swimmer. $\Gamma = 0.085$, $S = 10$, $C = 0.8$.

find that the swimmer has a tendency to crash into the wall. Similarly, if the puller is strong enough we find that the swimmer settles into a straight trajectory (with $Y(t) = 0$ if the swimmer is at the center of the channel, or with $Y(t)$ periodic in time due to strokes if the swimmer at some distance from the center, as is the case in Fig. 18).

In order to have a swimmer with a large enough stresslet, one way is to modify the force presented in section II A in the following way

$$\mathbf{F} = 2[\sin(\omega t) \cos(3\alpha) - (\beta + \cos(\omega t)) \cos(2\alpha)]\mathbf{n} \quad (21)$$

for a puller, where we recall that $\alpha = 2\pi s/L_0$ (s is the arclength and L_0 the perimeter), and

$$\mathbf{F} = 2[(-\beta + \sin(\omega t)) \cos(3\alpha) - \cos(\omega t) \cos(2\alpha)]\mathbf{n} \quad (22)$$

for a pusher (with $\beta > 0$). β monitors the strength of the swimmer nature (weak and strong pusher or puller).

Fig. 20 shows some typical cases where the strong pusher crashes into the wall and the strong puller settles into a straight trajectory. We also provide the corresponding values of the stresslet. It would be interesting in the future to analyze in more details this problem in order to determine the stresslet critical amplitude above which we have a transition from navigation to crashing/settling into a straight trajectory.

VIII. SUMMARY AND PERSPECTIVES

The current work presents a systematic study of hydrodynamics of microswimming by shape deformation (amoeboid swimming) in a planar microfluidic channel. By studying the coupling of shape change and wall interaction, we discovered several new features of microswimming. It is shown that the navigating mode of AS explores 80% ~ 95% of the available lateral space in the channel, and that the velocity behaves in a non monotonic way as a function of confinement. The dissipation structures reveal that the walls play an important role to enhance the swimming speed, provided the swimmer has enough space to fully deploy its shape. We have reported on scaling of the velocity with the force and found that the velocity is quadratic with the force at small enough force, and attains a plateau at large enough force. The nature of AS is found to be not an intrinsic property, but depends on environment, such as the strength of confinement.

Several other questions deserve future considerations. Of particular importance is the study of the wall compliance effect [43]. Indeed, many eukaryotic cells *in vivo* (e.g. cells of the immune system, cancerous cells...) move in soft tissues where cells are often in interstices, in between other cells and extracellular matrix. Therefore, the confinement is not fixed in time but varies in response to stresses created by the cells. A basic representation of this effect is to consider that the bounding walls have a

certain compliance. It would be important to see if the compliance can help enhance the swimmer speed by increasing confinement, since we have seen in this paper that the speed attains a maximum (and then a decline) because the rigid boundaries do not allow the swimmer to deploy fully its shape deformation. Another important issues is to study the collective behaviors. For example, during wound healing and cancer spreading (to name but few examples) cells move in a concerted fashion. It would be thus important to analyze if collective behaviors could emerge from the study of multiswimmers, such as special patterns, synchronization, and so on. Finally, *in vivo* cells move in complex visco-elastic materials, and it will be an important issues in the future to analyze AS in a complex medium. The immersed boundary method is a very good candidate in order to extend it in the future to the problem of locomotion in complex media.

IX. ACKNOWLEDGMENTS

H.W. thank Prof. S. Jung (Virginia Tech) for the helpful discussion on the experimental details. C.M., A.F., M.T., and H.W. were supported by CNES and ESA. S.R. and P.P. acknowledge support from ANR. All the authors acknowledge the French-Taiwanese ORCHID cooperation grant. W.-F. H., M.-C.L., and C.M. thank the MoST for a support allowing initiation of this project.

Appendix : Total force and total torque of tension force are zero

We have seen from general consideration that if the energy does not depend on position in space, then the total associated forces and torque are automatically zero. For interested readers we briefly give here an explicit proof. In 2D space, an amoeboid swimmer is represented by a 1D closed contour. For the force this is quite obvious since that force can also be written as

$$\mathbf{F}^{\text{ten}} = \frac{\partial(\zeta \mathbf{t})}{\partial s}$$

Therefore the integral over a contour is zero.

For the total torque \mathbf{T}^{tot} along the perimeter of amoe-

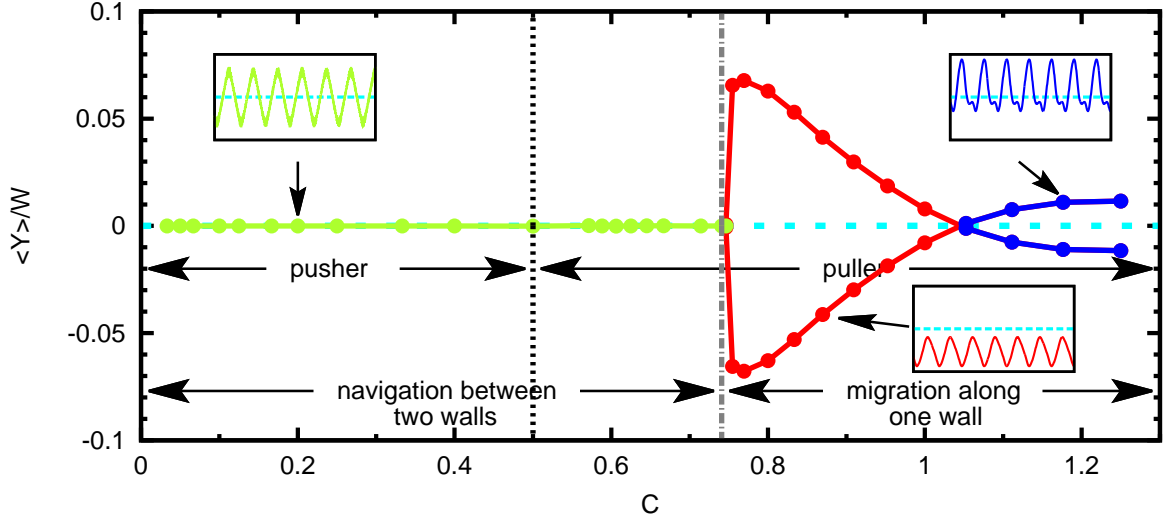


FIG. 19: (Color online) Average position along Y as a function of confinement. $\Gamma = 0.085$, $S = 10$.

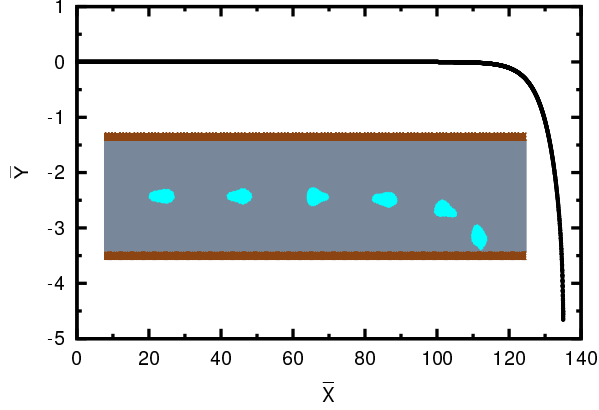


FIG. 20: (Color online) A trajectory showing a swimmer crashing into the wall. $\Gamma = 0.085$, $S = 1$, $C = 0.167$.

boid swimmer, we have:

$$\begin{aligned}
 \mathbf{T}^{\text{tot}} &= \oint_{\partial\Omega} [\mathbf{r} \times \mathbf{F}^{\text{ten}}] ds \\
 &= \oint_{\partial\Omega} [(x - X_c)F_y^{\text{ten}} - (y - Y_c)F_x^{\text{ten}}] ds \\
 &= \oint_{\partial\Omega} \left[(x - X_c) \frac{\partial(\zeta t_y)}{\partial s} - (y - Y_c) \frac{\partial(\zeta t_x)}{\partial s} \right] ds \\
 &= \oint_{\partial\Omega} [(x - X_c)d(\zeta t_y) - (y - Y_c)d(\zeta t_x)] \\
 &= \oint_{\partial\Omega} \left[-\frac{\partial(x - X_c)}{\partial s}(\zeta t_y) + \frac{\partial(y - Y_c)}{\partial s}(\zeta t_x) \right] ds \\
 &= \oint_{\partial\Omega} [-t_x(\zeta t_y) + t_y(\zeta t_x)] ds \\
 &= 0
 \end{aligned}$$

-
- [1] E. Lauga and T. Powers, Rep. Prog. Phys. **72**, 096601 (2009).
- [2] D. Saintillan and M. Shelley, J. R. Soc. Interface **9**, 571 (2012).
- [3] L. J. Fauci and A. McDonald, Bull. Math. Biol. **57**, 679 (1995).
- [4] V. Kantsler, J. Dunkel, M. Polin, and R. E. Goldstein, Proc. Natl. Acad. Sci. U.S.A. **110**, 1187 (2013).
- [5] E. Lauga, W. R. DiLuzio, G. M. Whitesides, and H. A. Stone, Biophys. J. **90**, 400 (2006).
- [6] A. P. Berke, L. Turner, H. C. Berg, and E. Lauga, Phys. Rev. Lett. **101**, 038102 (2008).
- [7] A. Sokolov and I. S. Aranson, Phys. Rev. Lett. **103**, 148101 (2009).
- [8] K. Drescher, K. C. Leptos, I. Tuval, T. Ishikawa, T. J. Pedley, and R. E. Goldstein, Phys. Rev. Lett. **102**, 168101 (2009).
- [9] J. S. Guasto, K. A. Johnson, and J. P. Gollub, Phys. Rev. Lett. **105**, 168102 (2010).
- [10] K. Drescher, R. E. Goldstein, N. Michel, M. Polin, and I. Tuval, Phys. Rev. Lett. **105**, 168101 (2010).
- [11] S. Jana, S. H. Um, and S. Jung, Phys. Fluid **24**, 041901 (2012).
- [12] P. Zhang, S. Jana, M. Giarra, P. Vlachos, and S. Jung, Eur. Phys. J. Spec. Top. **224**, 3199 (2015).
- [13] L. Zhang, J. J. Abbott, L. Dong, B. E. Kratochvil, D. Bell, and B. J. Nelson, Appl. Phys. Lett. **94**, 064107 (2009).
- [14] W. F. Paxton, K. C. Kistler, C. C. Olmeda, A. Sen, S. K. St. Angelo, Y. Cao, T. E. Mallouk, P. E. Lammert, and

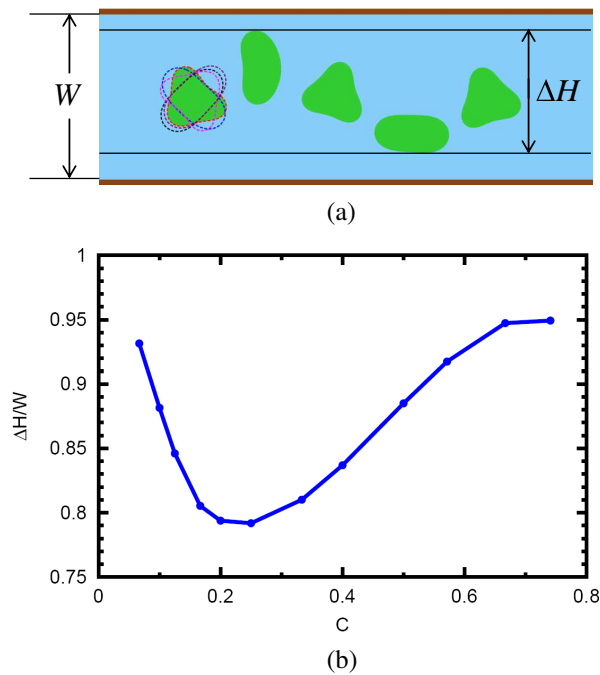


FIG. 21: (Color online) (a) The definition of height difference ΔH scanned by a navigating swimmer. (b) The scanned space for different confinements ($\Gamma = 0.085$, $S = 10$).

- V. H. Crespi, *J. Am. Chem. Soc.* **126**, 13424 (2004).
- [15] J. Thronsen, *Norw. J. Bot.* **16**, 161 (1969).
- [16] D. D'Ambrosio and F. Sinigaglia, *Cell Migration in Inflammation and Immunity* (Springer, 2004).
- [17] F. Entschladen and K. S. Zänker, *Cell Migration: Signalling and Mechanisms* (Karger Medical and Scientific Publishers, 2009).
- [18] T. Lämmermann, B. L. Bader, S. J. Monkley, T. Worbs, R. Wedlich-Soldner, K. Hirsch, M. Keller, R. Forster, D. R. Critchley, R. Fassler, et al., *Nature* **453**, 51 (2008).
- [19] Y.-J. Liu, M. Le Berre, F. Lautenschläger, P. Maiuri, A. Callan-Jones, M. Heuzé, T. Takaki, R. Voituriez, and M. Piel, *Cell* **160**, 659 (2015).
- [20] R. J. Hawkins, M. Piel, G. Faure-Andre, A. Lennon-Dumenil, J. Joanny, J. Prost, and R. Voituriez, *Phys. Rev. Lett.* **102**, 058103 (2009).
- [21] N. P. Barry and M. S. Bretscher, *Proc. Natl. Acad. Sci. U.S.A.* **107**, 11376 (2010).
- [22] M. Bergert, A. Erzberger, R. A. Desai, I. M. Aspalter, A. C. Oates, G. Charras, G. Salbreux, , and E. K. Paluch, *Nat. Cell Biol.* **17**, 524 (2015).
- [23] J. E. Avron, O. Gat, and O. Kenneth, *Phys. Rev. Lett.* **93**, 186001 (2004).
- [24] T. Ohta and T. Ohkuma, *Phys. Rev. Lett.* **102**, 154101 (2009).
- [25] T. Hiraiwa, K. Shitaraa, and T. Ohta, *Soft Matter* **7**, 3083 (2011).
- [26] F. Alouges, A. Desimone, and L. Heltai, *Math. Models Methods Appl. Sci.* **21**, 361 (2011).
- [27] M. Arroyo, L. Heltai, D. Millán, and A. DeSimone, *Proc. Natl. Acad. Sci. U.S.A.* **109**, 17874 (2012).
- [28] A. Vilfan, *Phys. Rev. Lett.* **109**, 128105 (2012).
- [29] J. Loheac, J.-F. Scheid, and M. Tucsnak, *Acta Appl. Math.* **123**, 175 (2013).
- [30] A. Farutin, S. Rafai, D. K. Dysthe, A. Duperray, P. Peyla, and C. Misbah, *Phys. Rev. Lett.* **111**, 228102 (2013).
- [31] H. Wu, M. Thiébaud, W.-F. Hu, A. Farutin, S. Rafai, M.-C. Lai, P. Peyla, and C. Misbah, *Phys. Rev. E* **92**, 050701 (2015).
- [32] M. Thiébaud and C. Misbah, *Phys. Rev. E* **88**, 062707 (2013).
- [33] W.-F. Hu, Y. Kim, and M.-C. Lai, *J. Comput. Phys.* **257**, 670 (2014).
- [34] E. M. Purcell, *Am. J. Phys.* **45**, 3 (1977).
- [35] B. Kaoui, G. Ristow, I. Cantat, C. Misbah, and W. Zimmermann, *Phys. Rev. E* **77**, 021903 (2008).
- [36] C. Pozrikidis, *Boundary Integral and Singularity Methods for Linearized Viscous Flow* (Cambridge University Press, 1992).
- [37] I. Cantat, K. Kassner, and C. Misbah, *Eur. Phys. J. E* **10**, 175 (2003).
- [38] F. H. Harlow and J. E. Welch, *Phys. Fluids* **8**, 2182 (1965).
- [39] L. N. Trefethen, *Spectral methods in MATLAB* (SIAM, Philadelphia, 2000).
- [40] B. U. Felderhof, *Phys. Fluids* **22**, 113604 (2010).
- [41] L. Zhu, E. Lauga, and L. Brandt, *J. Fluid Mech.* **726**, 285 (2013).
- [42] A. Bilbao, E. Wajnryb, S. A. Vanapalli, and J. Blawdziewicz, *Phys. Fluids* **25**, 081902 (2013).
- [43] R. Ledesma-Aguilar and J. M. Yeomans, *Phys. Rev. Lett.* **111**, 138101 (2013).
- [44] A. Acemoglu and S. Yesilyurt, *Biophys. J.* **106**, 1537 (2014).
- [45] B. Liu, K. S. Breuer, and T. R. Powers, *Phys. Fluids* **26**, 011701 (2014).
- [46] See Supplementary Information.
- [47] R. Nosrati, A. Driouchi, C. M. Yip, and D. Sinton, *Nat. Commun.* **6**, 8703 (2015).
- [48] A. Farutin, H. Wu, W.-F. Hu, M. Thiébaud, S. Rafai, M.-C. Lai, P. Peyla, and C. Misbah (2016), unpublished Manuscript.
- [49] M. J. Lighthill, *Mathematical Biofluidynamics (CBMS-NSF Regional Conference Series in Applied Mathematics)* (SIAM, 1975).
- [50] E. M. Purcell, *Proc. Natl. Acad. Sci. U.S.A.* **94**, 11307 (1997).
- [51] L. E. Becker, S. A. Koehler, and H. A. Stone, *J. Fluid Mech.* **490**, 15 (2003).
- [52] A. Shapere and F. Wilczek, *Phys. Rev. Lett.* **58**, 2051 (1987).
- [53] J. Koiller and J. Delgado, *Rep. Math. Phys.* **42**, 165 (1998).
- [54] A. Najafi, S. S. H. Raad, and R. Yousefi, *Phys. Rev. E* **88**, 045001 (2013).
- [55] If the membrane becomes unstuck from the cortex, the intercellular pressure is able to push the membrane into a hemispherical blister, known as a bleb.
- [56] Note that in Ref. [30] we have also explored a large number of harmonics without affecting the essential results, lending support to the present simplifications.